Preliminary study of selective contacts for hot carrier solar cells

Soline Boyer-Richard, Fei Fan, Nicolas Chevalier, Antoine Létoublon, Alexandre Beck, Karine Tavernier, Shalu Rani, Daniel Suchet, Andrea Cattoni, Laurent Lombez, et al.

EPJ Photovoltaics **15**, 38 (2024)

https://doi.org/10.1051/epjpv/2024031

Available online at:
www.epj-pv.org

Special Issue on 'Advances in French Photovoltaic Research in 2023', edited by Mohamed Amara, Thomas Fix, Jean-Paul Kleider, Judikaël Le Rouzo and Denis Mencaraglia

ORIGINAL ARTICLE OPEN ACCESS

Preliminary study of selective contacts for hot carrier solar cells

Soline Boyer-Richard[1,*], Fei Fan[1], Nicolas Chevalier[1], Antoine Létoublon[1], Alexandre Beck[1], Karine Tavernier[1], Shalu Rani[2], Daniel Suchet[2], Andrea Cattoni[3], Laurent Lombez[4], and Olivier Durand[1]

[1] Université de Rennes, INSA Rennes, CNRS, Institut FOTON - UMR 6082, 35000 Rennes, France
[2] IPVF SAS, UMR IPVF 9006, CNRS, Ecole Polytech, Inst Polytech Paris, PSL Chim, 91120 Palaiseau, France
[3] Univ Paris Saclay, Univ Paris Sud, CNRS, Ctr Nanosci & Nanotechnol C2N, 91120 Palaiseau, France
[4] LPCNO, INSA CNRS UPS, 135 Ave Rangueil, 31077 Toulouse, France

Received: 15 March 2024 / Accepted: 4 September 2024

Abstract. Hot carrier solar cells are a concept of photovoltaic devices, which offers the opportunity to harvest solar energy beyond the Shockley-Queisser limit. Unlike conventional photovoltaic devices, hot carrier solar cells convert excess kinetic energy into useful electrical power rather than losing it through thermalisation mechanisms. To extract the carriers while they are still "hot", efficient energy-selective contacts must be developed. In previous studies, the presence of the hot carrier population in a p-i-n solar cell based on a single InGaAsP quantum well on InP substrate at room temperature has been demonstrated by means of complementary optical and electrical measurements, leading to an operating condition for this device beyond the limit for classical device operation. This result allows to design a new generation of devices to increase the hot carrier conversion contribution. In this work, we study InGaAs/AlInAs type II heterojunction as a selective contact for a future hot carrier solar cell device epitaxially grown on (001) oriented InP substrate. Two p-i-n solar cells have been grown by molecular beam epitaxy on InP. The absorber is a 50 nm-thick InGaAs layer surrounded by AlInAs barriers, all lattice-matched to InP. Two architectures are compared, the first with two symmetrical AlInAs barriers and the second with a single InGaAs quantum well in the center of the n-side barrier to allow electron tunneling across the barrier. Electrical characteristics under laser illumination with two different wavelengths have been measured to investigate the effect of the selective contact compared to the barrier. This preliminary study of InGaAs/AlInAs-based selective contacts show that such III–V combination is adapted for a future hot carrier solar cell in the InP technology.

Keywords: Hot carrier solar cells / III-V quantum well / selective contact / InP

1 Introduction

Hot carrier solar cells (HCSC) are a concept of photovoltaic devices, which offers the opportunity to harvest solar energy beyond the limit (33%) set by the Shockley-Queisser model [1]. Unlike conventional photovoltaic devices, in hot carrier solar cells, the excess kinetic energy is converted into useful electric power rather than being lost through thermalization mechanisms The important feature of HCSC is not only the inhibition of the carrier cooling process [2], but also the extraction of the carriers before their thermalization [3]. In a hot carrier solar cell, the extraction of hot carriers occurs through contacts that accept only a very narrow range of energies, or at least above a sufficiently high energy barrier.

Therefore, energy selective contacts (ESCs) are crucial in preventing cold carriers in the contact from cooling the extracted hot carriers. This minimizes the entropy increase during carrier extraction [4,5].

Efficient ESCs can be realized by the purely quantum phenomenon of resonant tunneling [6]. This effect exists if electron-reflecting interfaces are closely spaced, i.e., with separations comparable to the electron wavelengths. Interference between different electron waves leads to discrete transmission peaks. So, one practical implementation of the requirement for a narrow range of contact energies is an energy selective contact based on resonant tunneling double barrier. Several III–V quantum wells double barrier resonant tunneling structures have been considered to obtain ESC. For example, modelling results have shown that, for a hot carrier cell based on an InN absorber, the optimum configuration for ESCs is constituted by an InN/$In_xGa_{1-x}N$ double-barrier structure [7].

* e-mail: soline.boyer@insa-rennes.fr

Among III-V classical QW structures, using the AlGaAs/GaAs system for ESC has also been studied by modelling [8], and experimentally [9,10].

InP based samples allow to reach lower bandgaps compared to GaAs. Hot carrier effect could be reached under 1 eV, taking advantage of the whole AM 1.5G solar spectrum. The presence of the hot carrier population in a p-i-n solar cell based on a single InGaAsP quantum well on InP substrate at room temperature has been demonstrated by means of complementary optical and electrical measurements [11], leading to working condition for this device above the limit for classical device operation. This result allows to design a new generation of devices for enhancing the hot carrier conversion contribution, provided that carrier extraction is improved. It is possible to envisage several different ESC structures within the context of this InP technology. A preliminary theoretical investigation was conducted by Cavassilas et al. [12], who proposed the use of AlGaAsSb barriers with an InGaAs quantum well lattice-matched to InP. Nevertheless, the fabrication of the quaternary barrier AlGaAsSb with an InGaAs quantum well for the purpose of performing an ESC is a challenging process, as it necessitates the precise control of numerous chemical elements to prevent mixing at the interface. To initiate the ESC study within the InP technology, we have elected to start with ternary alloys, with the objective of achieving enhanced interface control.

To gain further insight, an experimental study was conducted on AlInAs/InGaAs heterostructures lattice matched with InP as an ESC for electrons. Such AlInAs/InGaAs ternary system is already well studied for the development of strain-balanced Quantum Cascade Lasers [13,14]. The advantage of these materials is that they contain a common V element, which facilitates the growth by molecular beam epitaxy (MBE). The investigation of selective contacts is divided into two phases. The initial step involves the development of a semi-selective contact through the implementation of a type II alignment. Subsequently, the type II alignment is replaced by a double barrier resonant tunneling diode, maintaining the lattice matching of the AlInAs/GaInAs quantum well heterostructure with InP.

Two p-i-n solar cells have been epitaxially grown by MBE on (001)-oriented InP substrates. The absorber layer is a 50 nanometer-thick InGaAs layer surrounded by two AlInAs barriers, with every layer being lattice-matched to InP. The first sample features two symmetric AlInAs barriers while the second sample incorporates an InGaAs single quantum well positioned centrally within the AlInAs barrier, facilitating electron tunneling towards the n contact. To evaluate the ability of selective contacts based on the AlInAs/GaInAs ternary compound system on the further development of HCSC on InP wafers, this study presents conventional Dark I-V and Light I-V (under AM1.5G standard irradiance spectrum) characterization on circular top-contact solar cells. Moreover, electrical characterization has been conducted under two distinct wavelength laser illuminations to investigate the impact of a single quantum well (SQW) energy selective contact in comparison to a selective contact made with a barrier.

2 Material and methods

2.1 Sample epitaxial structure

The active layers of the initial structure, designated as BARRIER (Fig. 1a), are constituted by a 50-nanometer-thick InGaAs absorber surrounded by two 30 nanometer-thick AlInAs barriers. The upper contact layers of the heterostructure comprise a 100-nanometer heavily p-doped InGaAs contact layer on a p+ InGaAs layer. Accordingly, the selective contact for electrons in this initial structure is an AlInAs barrier, which works as a high-pass filter. The second structure (SQW) (Fig. 1b) is identical to the first in terms of its composition, while it includes a selective contact for electrons. This contact is composed of a SQW (13 nm-thick AlInAs/4 nm-thick InGaAs/13 nm-thick AlInAs). Both samples were grown by molecular beam epitaxy (MBE). The doping levels achieved for both the n+ (Si) and p+ (Be) layers were 8×10^{18} cm^{-3}. All the structures were grown on a (001) n+ InP substrate. This was done subsequently to the growth of a 300 nm-thick InGaAs buffer layer and a 50 nm n+ InP layer. The growth setup was a RIBER 2300 gas source MBE and the substrate growth temperature was 480 °C. The growth rates were 0.9 ML/s for InP, 0.53 ML/s for InGaAs and 1.18 ML/s for AlInAs. Figure 1 illustrates the planned band alignment at the n-side contact for both structures at T=0 K. The electron barrier height between AlInAs and InGaAs is 0.52 eV. An electron confined level is expected at $E_1 = 0.186$ eV (calculated with an effective mass model) in the 4 nm InGaAs quantum well.

2.2 Structural characterization

Two types of structural characterization are performed to evaluate the epitaxial quality of the samples prior to clean room technological steps. X-Ray diffraction (XRD) gives access to the different lattice parameters in the structure. XRD measurements were performed using a 5-circle Smartlab Rigaku diffractometer with Cu Kα1 radiation ($\lambda = 0.1540562$ nm) and equipped with a HyPix-3000 detector in high resolution mode using a front 2-bounce Ge (220) monochromator. Photoluminescence (PL) provides information about the energy levels involved in the sample. PL was performed at room temperature on the epitaxial samples (before technological steps) after removal of the InGaAs p+ layer by reactive ion etching (RIE) to avoid the electric field effect, with an excitation wavelength of $\lambda = 532$ nm and an integration time of 1 s.

2.3 Technological process

The technological fabrication process consists of widely used processes in the microelectronics domain. Here, four steps are required to define and insulate the front contact layer of the cells by mesa etching, as described in Figure 2. The first step consists of front electrode deposition (Ti/Au:20 nm/300 nm) by evaporation and patterning through photolithography and lift-off technique. A RIE is performed to remove the p+ heavily doped InGaAs

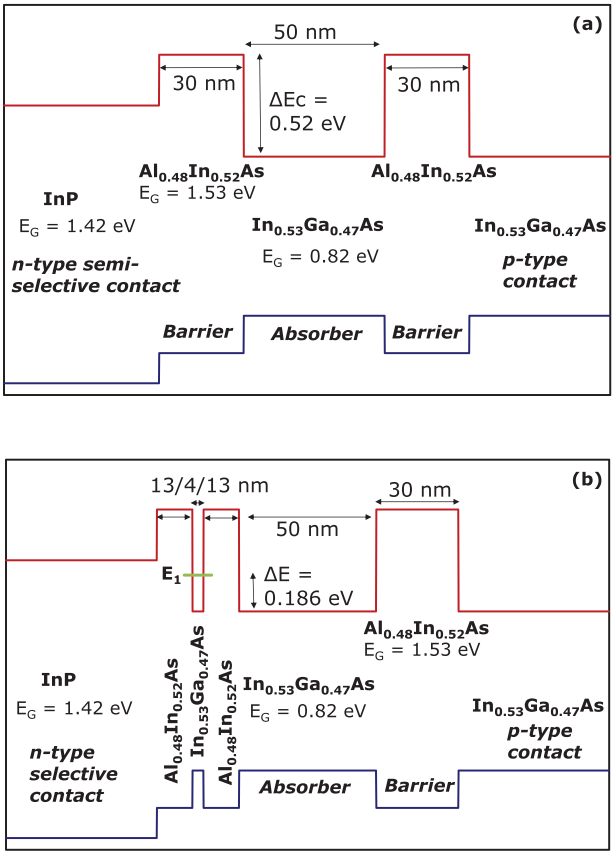

Fig. 1. Simplified energy band diagrams of ESC solar cells (a) BARRIER: with simple barriers and (b) SQW: with a QW in the n-side barrier. Energy levels are given at $T = 0\,\mathrm{K}$.

$(Ar/H_2/CH_4)$ using the deposited electrodes as a masking layer. The cells are then defined by a second photolithography followed by mesa wet etching down to the substrate. A dielectric layer (Si_3N_4) is then deposited by PECVD to avoid oxidation of AlInAs. This dielectric layer is patterned by photolithography and RIE to open a window and access the front electrode. Hence, contact pads are deposited to thicken the front electrode and to allow on-wafer characterization. Finally, a Ti/Au stack is deposited by evaporation on the backside of the n-doped InP substrate. Figure 3 summarizes the final samples structures, and a picture of the sample structure is presented in Figure 4.

2.4 Opto-electrical characterizations

Several types of optoelectrical measurements were performed on two 75 µm diameter circular diodes on each sample. New room temperature PL has been performed on both diodes, with a laser excitation wavelength of $\lambda = 532\,\mathrm{nm}$, under varying power, to characterize the electron energy levels involved in each diode. Classical current-voltage characteristics are obtained under solar simulator with an applied solar power density of $960\,\mathrm{W/m^2}$. Photocurrent measurements were performed with two lasers of different wavelengths, under varying incident power. The first laser wavelength is 1064 nm corresponding to an energy of 1.16 eV, therefore below the AlInAs bandgap, and the second wavelength is 532 nm corresponding to 2.32 eV, above the AlInAs bandgap. We demonstrate a better carrier extraction with the SQW sample than with the BARRIER one, especially with the 1064 nm laser. We performed 1D Schrödinger-Poisson simulations with SimWindows software [15] to model the carrier density along the structure under laser illumination.

3 Results and discussion

3.1 Structural characterization

Figure 5 presents X-ray diffraction results on the HCSC heterostructures. For the sample BARRIER, the main diffraction peaks coming from the InGaAs and AlInAs layers cannot be separated from the InP (004) substrate diffraction peak meaning that the heterostructure is almost lattice-matched as expected (Fig. 5a). Moreover, some thickness fringes are also observed on the left of the substrate peak. The slope of fringe order m as a function of the fringe position expressed into scale of the diffraction vector modulus $S = \frac{2\sin\theta}{\lambda}$ yields the corresponding thickness, around 45 nm-46 nm. This thickness is close to 50 nm nominal thicknesses of both InGaAs absorber and n+ InP layer (localized between the buffer layer and the AlInAs barrier). Considering now the sample SQW and as shown in Figure 5b, the InGaAs peak position has been measured at 6.80084 nm^{-1} which corresponds to an inter-reticular distance of 0.58816 nm. Therefore, considering the strain on the InP substrate, the In composition is equal to 0.548 (again, close to the required 0.53 amount of In). The thickness fringes are still present on the left of the InP (004) diffraction peak, giving 39 nm, a thickness a little bit lower than the nominal 50 nm-thick. A new thickness fringes system is also present at the right of the InP (004) diffraction peak, which gives a thickness around 14 nm. We attribute this contribution to the 13 nm nominally thick AlInAs barriers surrounding the InGaAs SQW.

3.2 Photoluminescence measurements

Two steps of PL were performed on the samples. The routine PL results on the epitaxial samples were so noisy that they are not shown here. A PL peak was measured at about 0.755 eV (1650 nm) from the BARRIER sample. This corresponds to the 0.74 eV bandgap energy expected for the $In_{0.53}Ga_{0.47}As$. Although the PL intensity is very low as compared to measurements obtained on conventional InGaAs/InP samples, due to the AlInAs barrier, the PL peak position confirms the good crystal quality of InGaAs. Under the same conditions, no PL signal was obtained for the SQW sample, which may be due to a lower crystal quality. Nevertheless, it was also processed as a diode considering the XRD results.

The second PL study has been performed on the center of the processed cells with a full etching of the InGaAs contact layer, allowing better results from the PL measurements. Figure 6 depicts the room temperature

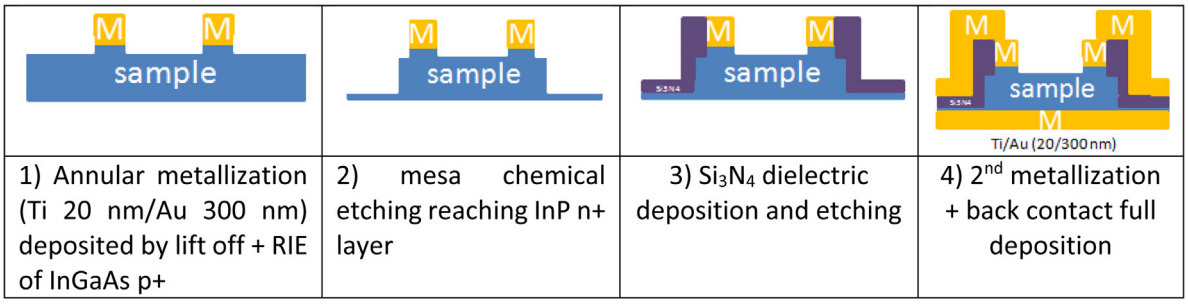

Fig. 2. Technological steps to obtain ESC samples.

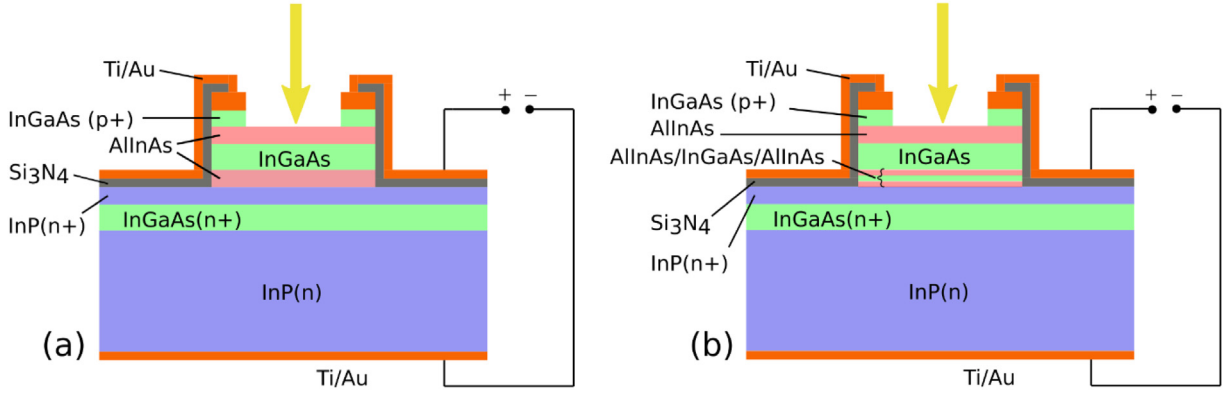

Fig. 3. Schematic view if the final structures (a) BARRIER and (b) SQW.

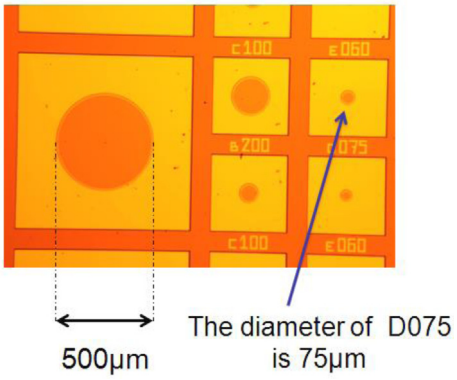

Fig. 4. Optical microscope view of the SQW sample.

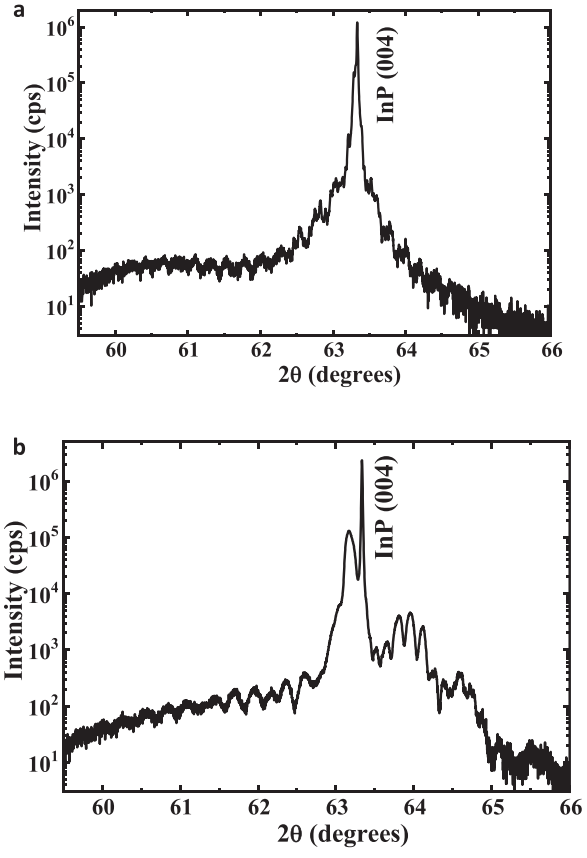

Fig. 5. XRD results for (a) the BARRIER sample and (b) the SQW sample.

PL results as a function of laser power for both samples. The PL threshold corresponds to the InGaAs bandgap (0.74 eV at room temperature) for both samples. The BARRIER sample exhibits a peak at approximately 0.77 eV, in accordance with the predicted energy of the bulk InGaAs 50 nm-thick absorption layer. The SQW sample exhibits two distinct peaks. The first is observed at approximately 0.76 eV, which is attributed to the bulk InGaAs layer. The second peak is observed at approximately 0.97 eV, which corresponds to the $E_1 - HH_1$ energy within the InGaAs 4 nm-thick quantum well. This result is consistent with the calculated confined levels (electron confined level $E_1 = 0.186$eV over the conduction band minimum, hole confined level $HH_1 = 25$ meV under the

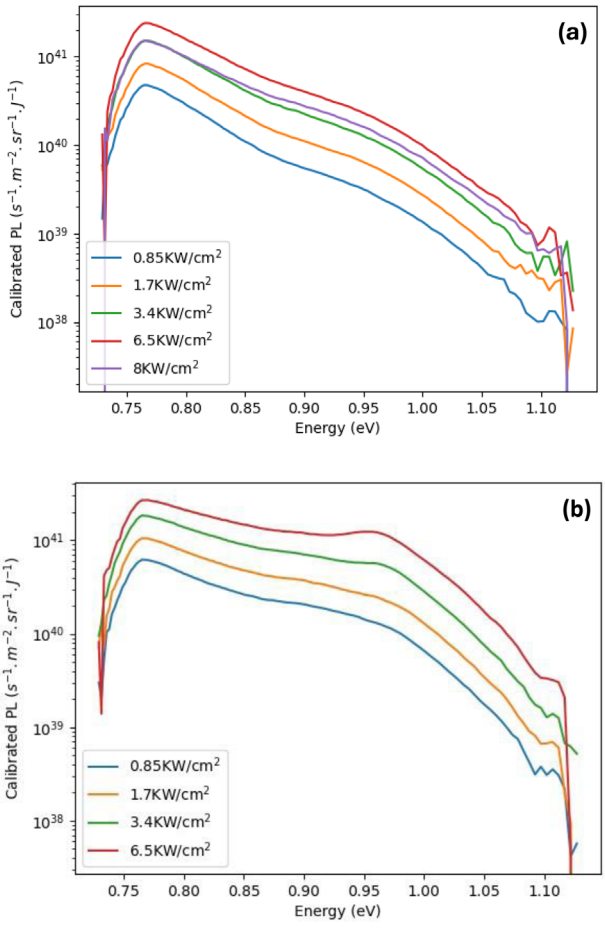

Fig. 6. Photoluminescence characteristics for (a) the BARRIER sample and (b) the SQW sample as a function of laser power.

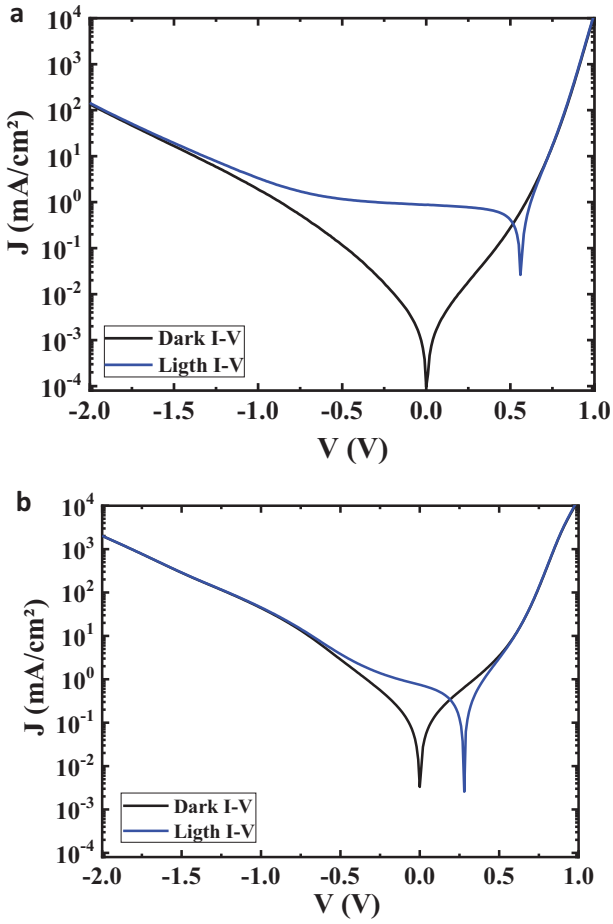

Fig. 7. J–V characteristics with logarithmic scale under AM1.5G illumination (a) BARRIER sample (b) SQW sample.

valence band maximum). It demonstrates the presence of the InGaAs quantum well in the AlInAs barrier, which can be used to extract electrons by tunnelling effect.

3.3 IV characteristics under AM1.5G solar illumination

J–V measurements have been performed under dark condition and under solar simulator (AM1.5G without concentration) to investigate the opto-electrical characteristics of both diodes as shown in Figure 7. Table 1 summarizes the characteristics measured on the cells. The BARRIER cell displays a J_{SC} equal to 0.88 mA/cm^2 while the J_{SC} of the SQW cell is 0.75 mA/cm^2. Therefore, both are on the same order of magnitude. The values of V_{OC} are respectively 0.56 V and 0.28 V for BARRIER cell and SQW cell. Indeed, with an InGaAs absorber, low values of V_{OC} were expected due to a bandgap of 0.74 eV. The V_{OC} of BARRIER is two times larger than the V_{OC} of SQW. The low values of the V_{OC} and the poor fill factor (FF) obtained for SQW are attributed to a low shunt resistance likely due to defects in the structure, according to the structural characterization. Of course, compared to the theoretical efficiency value for InGaAs (0.74 eV), which is around 22.5% according to the Shockley-Queisser limits, the efficiency measured in both cells is rather low. However, the presence of barriers in the structures can affect the efficiency of such devices. Nevertheless, obtaining such solar cells characteristics with presence of barriers in the structure is already an important result since the aim of the present study is focused on the development of selective contact for the subsequent development of HCSC; hence we performed laser photocurrent measurements to better understand how the SQW affects the characteristics of these cells.

3.4 Photocurrent under laser excitation

Photocurrent measurements were performed with laser excitation at two different wavelengths: 532 nm and 1064 nm, which correspond respectively to photons energy of 2.33 eV and 1.16 eV at room temperature. Figures 8b and 8c present the J–V curves obtained on the BARRIER cell under 532 nm and 1064 nm laser excitations for different incident powers. Figures 8b and 8d display the same curves for the SQW cell. Considering the BARRIER cell, excitation at a 1064 nm wavelength (Fig. 8c) is not absorbed by the InGaAs absorber: a very low current is obtained even with a strong power. However, the short circuit current is almost increased 100 times with the 532 nm laser (Fig. 8a) as compared to the J_{SC} obtained with the 1064 nm laser (Fig. 8c) with the same incoming power

Table 1. Solar cell characteristics under AM1.5G illumination.

	V_{OC} (V)	J_{SC} (mA/cm^2)	FF	P_{max} (mW)	η	Light R_s (Ω cm^2)	Light R_{sh} (Ω cm^2)
HCSC – BARRIER	0.56	0.88	53.07%	1.15×10^{-5}	0.47%	136	2700
HCSC – SQW	0.28	0.75	32.86%	3.03×10^{-6}	0.12%	222	543

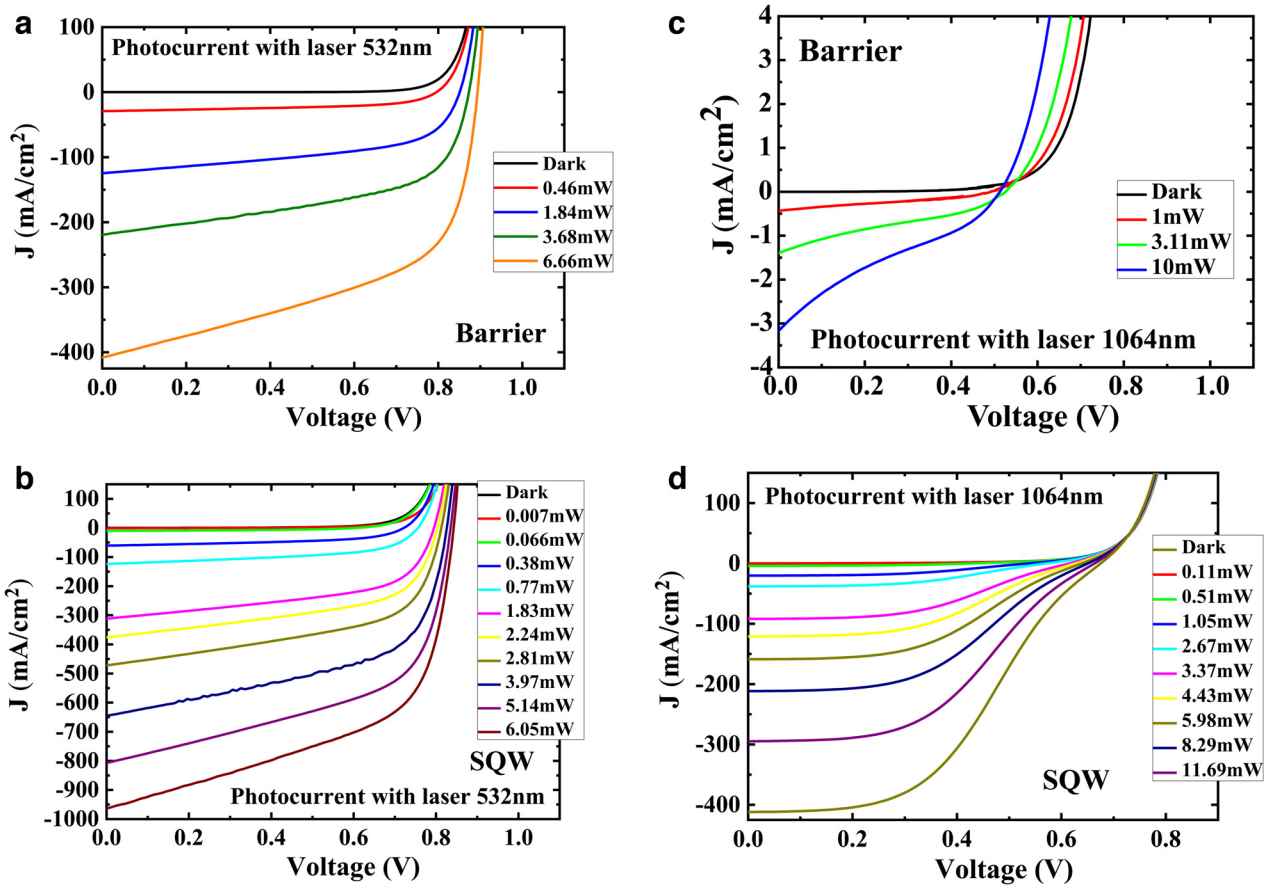

Fig. 8. *J–V* characteristics under laser illumination for different laser powers, in linear scale. (a)(b) 532 nm laser/(c)(d) 1064 nm laser/(a)(c) BARRIER Sample/(b)(d) SQW sample.

of 3 mW. The opto-electrical characteristics measured on the SQW cell are strongly different for the 1064 nm laser as shown on Figure 8d, in comparison with the results obtained in the BARRIER cell. At this wavelength, the SQW cell exhibits good *I–V* characteristics: photogenerated carriers in InGaAs can be extracted and contribute to the photocurrent, contrary to the BARRIER cell case. The curves of Figure 8d (under 1064 nm) show a S-shape displaying two different regimes with a transition around 0.3 V, while Figure 8b shows classical *I–V* shape for an excitation wavelength of 532 nm. The specific shape of the *I–V* curve under a 1064 nm (Fig. 8d) excitation can be explained by the selective contact. Indeed, for a low voltage, photogenerated electrons can travel across the barrier by tunnel effect if the confined level is adapted while the increase of voltage limits this effect and reduces the current. A specific "S-shape" is observed which limits the V_{OC} obtained under a 1064 nm excitation.

Figure 9 shows that the V_{OC} increases as a logarithmic function of laser power for the 532 nm laser for both samples. With a 1064 nm excitation, this tendency is only observed for the SQW cell while it remains almost constant for BARRIER cell (with very low corresponding J_{SC}). This behavior is also observed when measuring the V_{OC} variation of classical solar cells as a function of light concentration [16]. To compare the behavior of V_{OC} with laser power, therefore with concentration, we estimate the laser power corresponding to the same short circuit current as obtained under 1 sun. J_{SC} equals to 0.88 mA/cm^2 for the BARRIER cell under AM 1.5G. The nearest J_{SC} value obtained under laser illumination is 0.81 mA/cm^2 with 532 nm photoexcitation under laser power of 0.015 mW. Assuming that J_{SC} is proportional to light concentration, we estimate that a laser power of 0.015 mW corresponds to 0.92 sun. Using the same relation, a laser power of 1 mW would correspond to a concentration of 61.3 suns. Applying

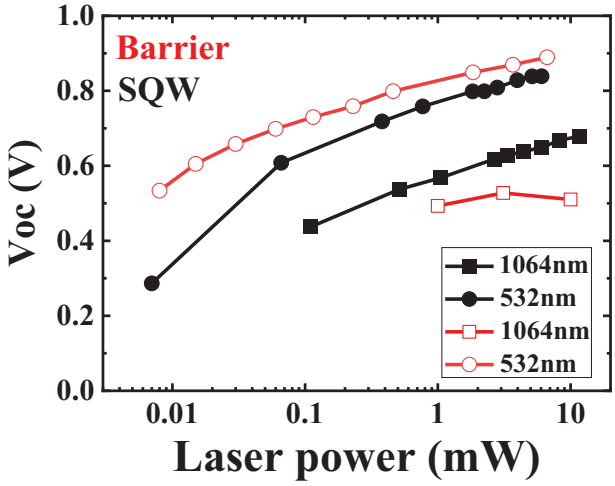

Fig. 9. Open circuit voltage under laser illumination as a function of laser power for both samples and both wavelengths.

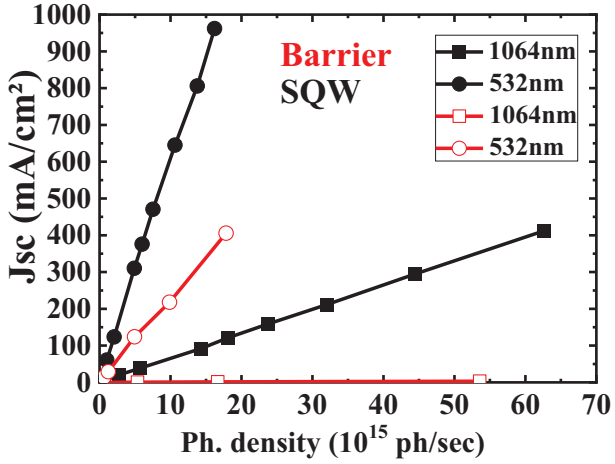

Fig. 10. Short circuit current density under laser illumination as a function of photon density for both samples and both wavelengths.

the same calculation to SQW cell, the J_{SC} equals to $0.75\,mA/cm^2$ for the Barrier cell under AM 1.5G corresponding to 1 sun, we can get the concentration for J_{SC} ($0.87\,mA/cm^2$) with 532 nm (laser power=0.007 mW) photoexcitation, which is 1.16 sun, that is to say a laser power of 1mW is equivalent to 165.7 suns. For the SQW cell, V_{OC} is reduced under the 1064 nm laser illumination compared to 532 nm laser illumination, but the two curves remain parallel.

Considering J_{SC} on Figure 10, we can see that the SQW cell displays a larger J_{SC} than the BARRIER cell under the 532 nm wavelength excitation (SQW cell has a J_{SC} about two times larger than the BARRIER cell one), suggesting that more current flows through the single quantum well. J_{SC} varies almost linearly as a function of laser power. This behavior is the same as observed for solar cells under

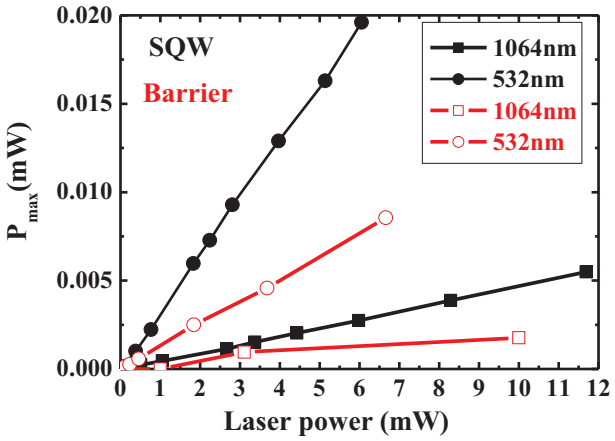

Fig. 11. Maximum power under laser illumination as a function of laser power for both samples and both wavelengths.

varying concentration [16]. Maximum electric power follows the same trend than J_{SC} for each set of measurement as shown in Figure 11. To compare them, we extract conversion efficiency from the slopes of these curves. To obtain the conversion efficiency, we need to know the surface area of the ellipse which comes from the NA 0.22 fiber to produce the exciting light. The ellipse has diameters of 400 µm by 200 µm, while the diode has a diameter of only 75 µm. So, we can estimate the ratio of the light power illuminating the diode over the output power from the fiber, which equals to the ratio of the surface of the diode over the area of the ellipse, that is 7%.

Therefore, for the BARRIER cell under 532 nm photoexcitation, conversion efficiency is obtained by dividing the slope of the linear curve (0.0013) by the ratio of the inserted light power over the output power (7%). We obtain a conversion efficiency of 1.86% at 532 nm. The 1064 nm photons are not absorbed, or only by barrier layers and thus very low power is obtained and no efficiency is calculated. Using the same procedure, for SQW cell under 1064 nm photoexcitation, conversion efficiency equals to 0.71%, while under 532 nm photoexcitation, the slope of the linear curve increases to 0.003, leading to a conversion efficiency of 4.3%. For the 532 nm excitation, the conversion efficiency obtained with the SQW cell is more than twice the one of the BARRIER cell, showing an important contribution of the quantum well channel even for high energy photons.

3.5 Simulation results under laser excitation

To better understand the observations, SimWindows (a free 1D semiconductor device simulation tool) calculations have been performed considering laser excitation at both wavelengths. Figure 12 presents the carrier concentration along the devices for both samples and both wavelengths. Figure 12a shows the carrier concentration as a function of laser power for the 532 nm wavelength for the BARRIER cell. For a laser power of 10 mW, the n-type concentration reaches almost 5×10^{17} cm^{-3}, about the

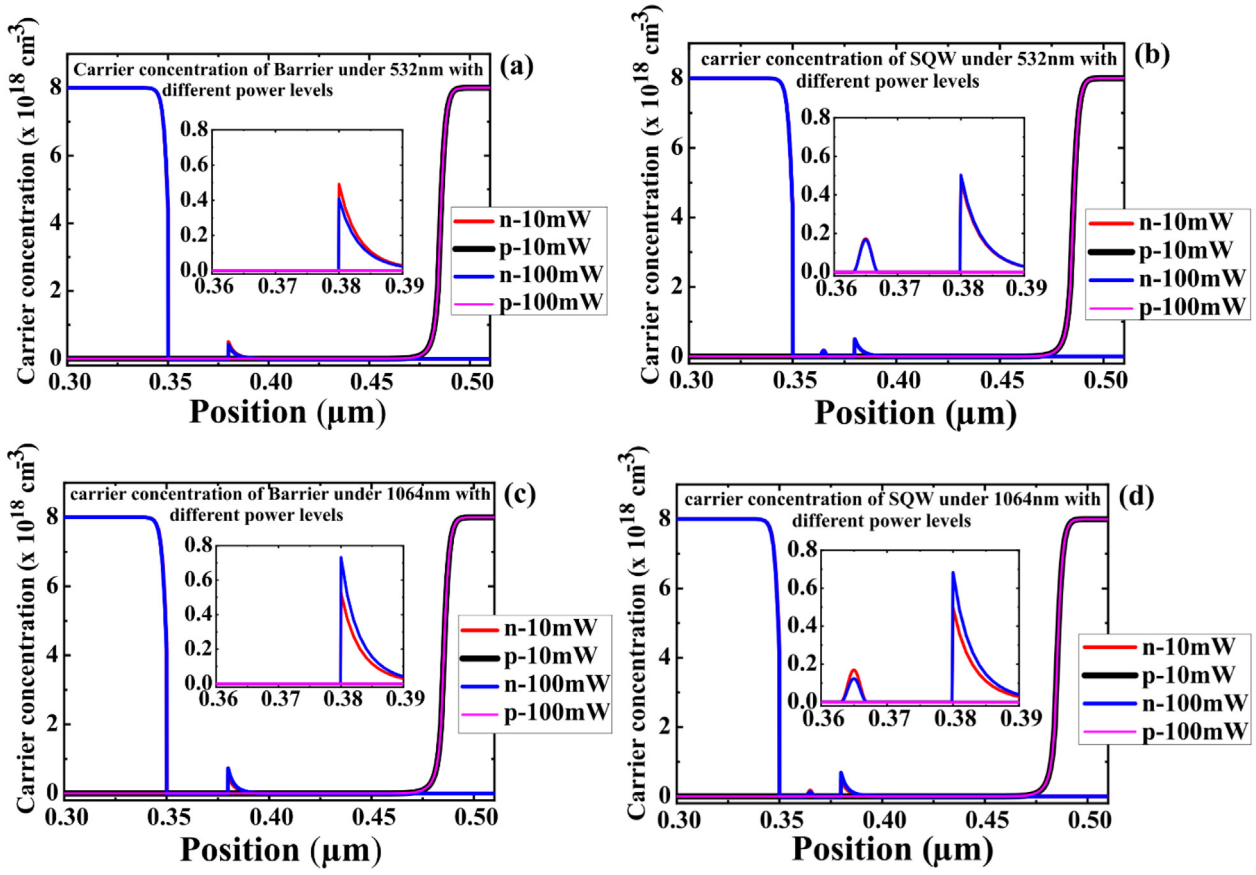

Fig. 12. Simulated carrier concentration as a function of the position for the 2 samples with different laser excitation (a)(b) 532 nm laser/(c)(d) 1064 nm laser/(a)(c) BARRIER sample/(b)(d) SQW sample.

same value as the one simulated under AM1.5G excitation. When the laser power increases, the carrier concentration decreases, showing that the carriers are easily extracted, since the increase of the mean carrier energy with laser power helps the carrier extraction to overcome the barrier. Conversely, for the 1064 nm laser (Fig. 12c), one can observe that the carrier concentration in the InGaAs absorption layer increases with the laser power, reaching 7×10^{17} cm^{-3}. The AlInAs barrier clearly blocks electrons. Only electrons with high enough energy can cross the barrier, explaining the poor electrical characteristics obtained with this sample at 1064 nm wavelength.

Figure 12b shows the carrier concentration for a 532 nm wavelength laser. It presents the same shape as under AM1.5G solar spectrum, for a laser power of 10 mW as well as 100 mW. The carrier concentration reaches 2×10^{17} cm^{-3} in the well and is maximal in the absorber layer with a value of 5×10^{17} cm^{-3}. Contrary to the case of the BARRIER cell, the carrier concentration does not depend on the laser power: more carriers are photogenerated with a higher laser power but they are efficiently extracted and contribute to the photocurrent. For 10 mW laser power, the mean carrier energy is probably lower but carriers are also extracted by the SQW confined level. Figure 12d shows the carrier concentration for a 1064 nm wavelength laser. At high laser power, the electron concentration increases in the absorber layer while it decreases in the SQW. The average electronic energy is expected to be higher and does not correspond anymore to the confined electronic level in the well, reducing the carrier extraction efficiency. Therefore, tunneling seems to be more efficient for a low laser power.

These simulations help to understand the photocurrent results: tunneling fully explains the better electrical characteristics of the SQW sample with the 1064 nm laser. However, the simulation results for higher laser power regime could not be reached experimentally so the expected decrease of tunneling with laser power could not be confirmed.

4 Conclusions

Two types of electron selective contacts have been investigated for the extraction of carriers in an InGaAs/InP solar cell in the framework of the development of HCSC in the InP technology: a semi-selective AlInAs barrier and a selective AlInAs/InGaAs single quantum well. Both samples have been grown by gas source MBE, which enabled the formation of abrupt interfaces with ternary alloys epitaxially grown on (001)-oriented InP substrate. Structural characterizations were performed using X-ray diffraction which indicated that the heterostructures

exhibited near lattice-matching. Subsequently, the relevance of using ESC from the AlInAs/InGaAs ternary system, using either selective or semi-selective contacts for further HCSC development on InP substrates, was investigated through opto-electrical characterization. Photoluminescence measurements yielded the expected result, confirming the presence of a quantum well confined level in the AlInAs/InGaAs single quantum well. Despite the poor electrical characteristics observed in both samples under solar illumination, since the solar cells were not yet optimized, the photocurrent results obtained under laser excitation provide a promising validation for the AlInAs/GaInAs ESC design. In particular, the photocurrent results obtained using two different lasers are larger for the SQW case, displaying higher efficiencies for both wavelengths. While further steps are required to adapt the confined level to hot carriers to allow higher V_{OC}, these results pave the way for future development of efficient HCSC on InP substrates, with an architecture better suited to the solar spectrum harvesting.

Acknowledgments

The authors acknowledge RENATECH+ (French Network of Major Technology Centers) for technological support. The authors thank Yoan Léger for technical help to perform laser photocurrent measurements and useful discussions.

Funding

This work is supported by the French National Research Agency project ICEMAN (Grant no. ANR-19-CE05-0019).

Conflicts of interest

The authors have nothing to disclose.

Data availability statement

This article has no associated data generated and/or analyzed.

Author contribution statement

Design of the selective contact was conducted by A. Cattoni, L. Lombez, O. Durand and S. Boyer-Richard in the framework of ICEMAN French ANR project. Sample growth and structural characterization were performed by N. Chevalier and A. Létoublon. Technological steps were conducted by K. Tavernier, A. Beck and F. Fan. Photoluminescence experiments were performed by S. Rani and D. Suchet. Solar cell experiments were conducted by F. Fan, and S. Boyer-Richard, and interpreted with the help of D. Suchet. The supervision of the project was ensured by O. Durand. The writing of the manuscript was performed by S. Boyer-Richard and O. Durand and proof reading by all co-authors.

References

1. G. Conibeer, J.-F. Guillemoles, F. Yu, H. Levard, Hot carrier solar cells, in *Advanced Concepts in Photovoltaics*, edited by A. Nozik, G. Conibeer, M.C. Beard (The Royal Society of Chemistry, 2014). https://doi.org/10.1039/9781849739955-00379
2. G. Conibeer, Hot carrier cells: an example of third generation photovoltaics, Proc. SPIE **8256**, 82560Z (2012). https://doi.org/10.1117/12.916520
3. A. Le Bris et al., Hot carrier solar cells: controlling thermalization in ultrathin devices, IEEE. J. Photovoltaics **2**, 506 (2012). https://doi.org/10.1109/JPHOTOV.2012.2207376
4. S.K. Shrestha, P. Aliberti, G.J. Conibeer, Energy selective contacts for hot carrier solar cells, Sol. Energy Mater. Sol. Cells **94**, 1546 (2010). https://doi.org/10.1016/j.solmat.2009.11.029
5. F. Gibelli, A. Julian, Z.J.L. Kao, J.-F. Guillemoles, Third generation hot carrier solar cells: paths towards innovative energy contacts structures, Proc. SPIE **9743**, 97430S (2016). https://doi.org/10.1117/12.2213562
6. S. Su, T. Liao, X. Chen, G. Su, J. Chen, Hot-carrier solar cells with quantum well and dot energy selective contacts, IEEE J. Quantum Electron. **51**, 1 (2015)
7. Y. Feng et al., Non-ideal energy selective contacts and their effect on the performance of a hot carrier solar cell with an indium nitride absorber, Appl. Phys. Lett. **100**, 053502 (2012). https://doi.org/10.1063/1.3680594
8. D. Suchet, Z. Jehl, Y. Okada, J.-F. Guillemoles, Influence of hot-carrier extraction from a photovoltaic absorber: an evaporative approach, Phys. Rev. Appl. **8**, 034030 (2017). https://doi.org/10.1103/PhysRevApplied.8.034030
9. S. Yagi, Y. Hijikata, Y. Okada, H. Yaguchi, Quantum well double barrier resonant tunneling structures for selective contacts of hot carrier solar cells, in *2011 37th IEEE Photovoltaic Specialists Conference* (2011), pp. 003309–003312. https://doi.org/10.1109/PVSC.2011.6186646
10. Z. Jehl et al., Hot carrier extraction using energy selective contacts and feedback on the remaining distribution, in *2018 IEEE 7th World Conference on Photovoltaic Energy Conversion (WCPEC) (A Joint Conference of 45th IEEE PVSC, 28th PVSEC & 34th EU PVSEC)* (2018), p. 1814. https://doi.org/10.1109/PVSC.2018.8548164
11. D.-T. Nguyen et al., Quantitative experimental assessment of hot carrier-enhanced solar cells at room temperature, Nat. Energy **3**, 236 (2018). https://doi.org/10.1038/s41560-018-0106-3
12. N. Cavassilas et al., Theoretical demonstration of hot-carrier operation in an ultrathin solar cell, Phys. Rev. Appl. **17**, 064001 (2022). https://doi.org/10.1103/physrevapplied.17.064001
13. M. Mikulicz et al., Enhancement of quantum cascade laser intersubband transitions via coupling to resonant discrete photonic modes of subwavelength gratings, Opt. Express **31**, 26898 (2023). https://doi.org/10.1364/OE.496261
14. G. Paz-Martínez et al., Comparison of GaN and InGaAs high electron mobility transistors as zero-bias microwave detectors, J. Appl. Phys. **132**, 134501 (2022). https://doi.org/10.1063/5.0111114

15. D.W. Winston, Physical Simulation of Optoelectronic Semiconductor Devices, Ph.D. thesis, University of Colorado, Boulder, USA (1996)
16. P. Singh, N.M. Ravindra, Temperature dependence of solar cell performance—an analysis, Sol. Energy Mater. Sol. Cells **101**, 36 (2012). https://doi.org/10.1016/j.solmat.2012.02.019

Cite this article as: Soline Boyer-Richard, Fei Fan, Nicolas Chevalier, Antoine Létoublon, Alexandre Beck, Karine Tavernier, Shalu Rani, Daniel Suchet, Andrea Cattoni, Laurent Lombez, Olivier Durand, Preliminary study of selective contacts for hot carrier solar cells, EPJ Photovoltaics **15**, 38 (2024)